Electronic Supplementary Material (ESI) for Physical Chemistry Chemical Physics.

Electronic Supplementary Information
Ammonia-modified Co(II) sites in zeolites: spin and electron density redistribution through the Co^{II}-NO bond

Adam Stępniewski[1], Mariusz Radoń[2], Kinga Góra-Marek[2] and Ewa Broclawik[1]*

[1]*Jerzy Haber Institute of Catalysis PAS,. Niezapominajek 8, 30-239 Krakow, Poland*
[2]*Faculty of Chemistry, Jagiellonian University, Ingardena 3, 30-060 Krakow, Poland*

I. Periodic simulations and extended cluster models

Ab-initio DFT calculations for periodic systems were performed using the Vienna ab-initio simulation package[S1-S4] (temporary access provided to one of Authors (AS) during STSM stays at Vienna University and Bratislava Comenius University within cooperation financed by the COST action CM1305).

The iterative solution of Kohn-Sham equations was carried out in a plane-wave basis set using the projector-augmented-wave (PAW) method of Blochl[S5], as adapted by Kresse and Joubert[S6]. The PBE generalized gradient approximation[S7] (GGA) was chosen to describe the exchange-correlation energy. Brillouin zone sampling was restricted to the gamma point. Smearing parameter σ for the Gaussian smearing of eigenstates was set to 0.01 eV. Geometry optimizations in a fixed-moment mode were performed with 400 eV cut-off energy. A conjugate-gradient algorithm[S8] was employed to optimize the potential minima. The atomic positions were considered as relaxed when all forces acting on atoms were less than 0.03 eV/Å. The electronic self-consistency cycle was terminated when the change in total energy was smaller than 10^{-8} eV/cell.

Simulations concerned the structure of cobalt exchanged chabazite with two Al atoms per a simulation cell containing 24 tetrahedral units (SiO_4 or AlO_4). Cobalt cation Co^{2+} was located either in six-member ring (6MR) or eight-member ring (8MR). All calculations were performed in a fixed-moment mode and for two spin states – singlet and triplet. Lattice parameters derived from experimental geometry of the highly siliceous form (SSZ-13) of chabazite[S9] ($R\bar{3}m$, a = 9.291 Å, α = 93.92°) were fixed. To avoid the undesired interaction between periodically repeated images of the cobalt center, the unit cell (a_1,a_2,a_3) was extended to a larger simulation cell (a,b,c) according to the following transformation of the lattice vectors: $a = a_1 + a_2$, $b = a_1 - a_2$, and $c = a_3$, resulting in the lattice parameters a = 12.682 Å, b = 13.581 Å, c = 9.291 Å, α = 90.00°, β = 95.74°, and γ = 90.00°. The smallest distance between atoms from the repeated cobalt centers is greater than 5 Å.

Two types of cobalt centers in chabazite were considered: i) the configuration with one NO ligand bound to cobalt, ii) nitric oxide and either two or three ammonia molecules co-bound to cobalt. Initial configurations for the simulations were based on previous studies[S10-S12] on the Al siting in zeolitic rings: e.g. Dedecek et al.[S10] reported Al-(O-Si)$_2$-O-Al distribution as frequently occurring in 6MR.The formation of the Al-(O-Si)$_3$-O-Al sequence in 8MR was suggested for mordenite framework. In our calculations Al-(O-Si)$_2$-O-Al sequence is present in the same hexagonal ring while the Al-(O-Si)$_3$-O-Al arrangement creates the cationic site in 8MR. The calculations converged to the triplet ground state for cobalt bonded with NO and accommodated in 6MR (Fig. S1). Part of the optimized periodic structure (marked by atom names in Fig. S1) served to construct the extended T12 clusters comprising one or two Al substitutions (with H atoms used to terminate dangling bonds) subjected to subsequent DFT optimization, electronic structure calculations and vibration analysis. Figs. S2 and S3 show the optimized geometries of the two extended clusters.

After co-adsorption of two NH_3 molecules the energetic order of cobalt locations points to 8MR (Fig. S2a). The ground state is the singlet for structure in 6MR and 8MR, the latter is favored by 5.9 kcal/mol. Bonding with third ammonia molecule is effectively only in 8MR (Fig. S2b), the calculations converged to singlet ground state (lying 6.1 kcal/mol below the triplet state).

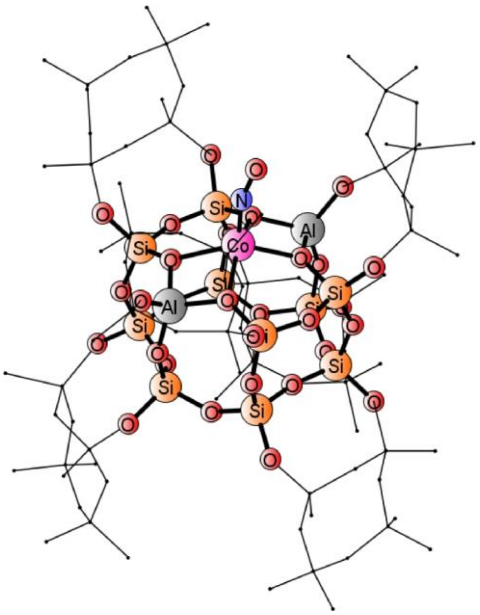

Fig. S1 Fragment of periodic structure for triplet-optimized coordination of a Co(II) cation with nitric oxide ligand in a six-member ring of chabazite. T atoms and oxygens included in T12 cluster marked by names. Silicon atoms are in orange, oxygen atoms in red, aluminum atoms in grey, cobalt atom in pink, and nitrogen atom in blue.

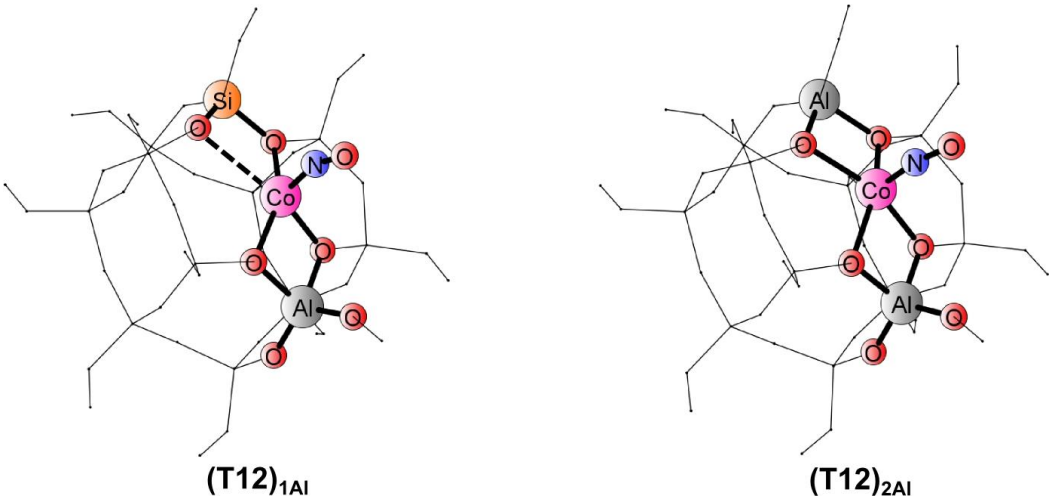

Fig. S2. Optimized geometries for cluster models **(T12)$_{1Al}$** and **(T12)$_{2Al}$** (in triplet states). Atoms in the part compatible to small (T1-based) cluster marked by names (other atoms shown schematically)

Table S1. The comparison of structural parameters, electron density distribution and NO stretching frequencies for the small $(\mathbf{a})_{\mathbf{T}}$ and extended (**T12)** models of the native Co(II) site (in triplet spin states); O1→ O_{Al}, O2 → O_{H2O} (in (**a**)) or $O_{Al/Si}$ (in $\mathbf{T_{12}}$)

	$\mathbf{(a)_T}$	$\mathbf{(T12)_{1Al}}$	$\mathbf{(T12)_{2Al}}$
	Angle (deg)		
Co-N-O	180.0	160.6	161.6
	Bond length (Å)		
Co-NO	1.69	1.70	1.70
N-O	1.14	1.14	1.15
$Co-O_1$	1.97; 1.97	1.95; 2.05	2.05; 2.23
$Co-O_2$	2,19; 2,19	2.19; 2.76	2.08; 2.19
	Electronic and vibrational properties		
Q_{Co} [a)]	+0.55	+0.56	+0.54
Q_{NO} [a)]	+0.22	+0.22	+0.18
ρ^{S}_{Co} [b)]	2,19	2.03	2.09
ρ^{S}_{NO} [b)]	0.43	0.35	0.43
$\Delta\nu_{NO}^{calc}$ (cm^{-1})	+74	+44	+28

[a)] from Mulliken populations; [b)] in spin minority

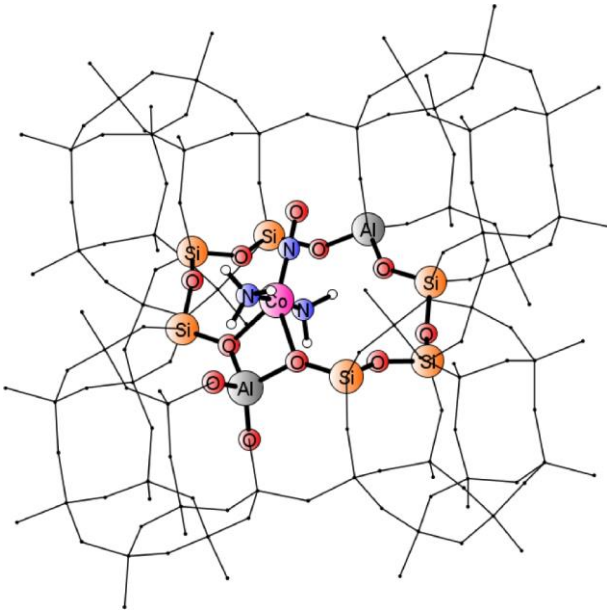

(a)

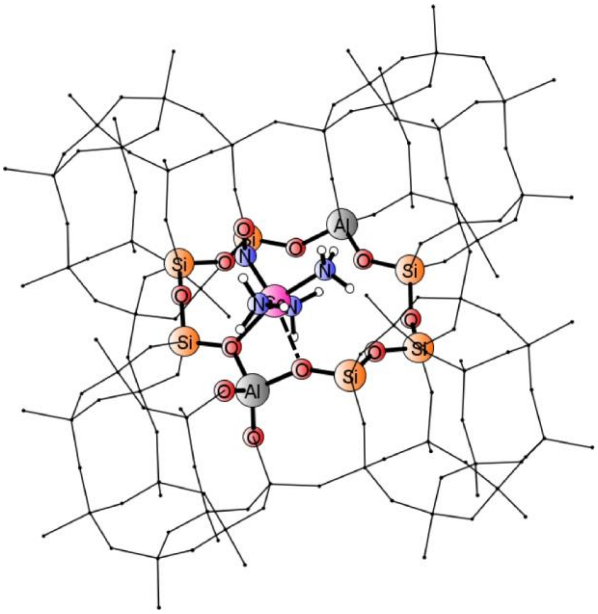

(b)

Fig. S3 Fragment of periodic structure for singlet-optimized coordination of a Co(II) cation with nitric oxide and two (a) or three (b) ammonia ligands in a eight-member ring of chabazite. Silicon atoms are in orange, oxygen atoms in red, aluminum atoms in grey, cobalt atom in pink, nitrogen atom in blue, and hydrogen atoms in white.

II. Selection of active space in CASSCF calculations and Valence Bond (VB)-like expansion of CASSCF wave function.

The active space was constructed in accord with standard rules for transition metal systems (ref. 48, main article). Thus, all molecular orbitals arising from $3d_{Co}$ and π^*_{NO} orbitals as well as π_{NO} and (lone pair) σ_{NO} orbitals were active. A double-shell orbital (d'_{Co}) was added for $d_{xz,Co}$, $d_{yz,Co}$ (the Co–N(O) bond being the local *z*-axis) and for every nonbonding d_{Co} orbital (doubly-occupied in the leading configuration). For $(\mathbf{a})_T$ and $(\mathbf{a^*})_T$ this approach leads to an active space of 14 active electrons in 13 active orbitals, denoted as (14,13). For $(\mathbf{a})_S$ and $(\mathbf{a^*})_S$ the appropriate active space is (14,14) one, *i.e.*, with one more double-shell orbital, due to one more d_{Co} orbital being doubly-occupied. For models $(\mathbf{b})_S$, $(\mathbf{b})_T$ and (**c**), due to the greater number of NH_3 co-ligands and favorable overlap of their lone pairs with one of the Co 3d orbitals, an additional covalent $Co–N_{NH3}$ interaction arises. To account for that, an occupied σ_{NH3} orbital (i.e., suitable combination of the NH_3 lone pairs) was made active, leading to the (16,14) active space. The choice of active space for all models is summarized in Table S4. Contour plots of the active orbitals can be found in Figures S5–S10.

Valence-bond (VB)-like expansion of CASSCF wave function in terms of resonance structures was performed analogously as in our previous study (ref. 13, main article), though with several noticeable improvements. First, the Pipek-Mezey method[S13] was employed for orbital localization (as in ref. 12, main article). From our experience with metal-nitrosyl complexes, the Pipek-Mezey method usually leads to a better localization than the previously applied Cholesky method. However, the usage of Pipek-Mezey localization in Molcas requires the symmetry to be switched off (although in our calculations the wave function remains appropriately symmetric and the energy is identical with and without the formal use of symmetry). Second, in the present approach all active orbitals are initially localized, which

leads to better separation of the π^*_{NO} and d'_{Co}, components than before (ref 13, main article). Note, however, that once all active orbitals are localized, the π_{NO}, π_{NO}^* orbitals convert into four 2p atomic orbitals (on N, O atoms). To restore the π_{NO}, π_{NO}^* orbitals and also improve the shape of the d_{Co}, d'_{Co} orbitals, the localized active orbitals are subsequently divided in two groups: the four mentioned atomic 2p orbitals (I) and the rest (II); and CASSCF calculations are repeated with orbital rotations only allowed within each group (I) or (II), but not between them. (The "supersymmetry" feature of the Molcas code was employed to restrict the orbital rotations.) The final orbitals obtained are within group (I): π_{NO} and π^*_{NO} orbitals; within group (II): d_{Co}, d'_{Co} as well as σ_{NO} and σ_{NH3} orbitals. The third difference compared with the previous work (ref. 13, main article) is that *all* configurations appearing in the expanded CASSCF wave function (not only the few most important ones) are analyzed by an automated counting of electrons in the π_{NO}, π_{NO}^* orbitals (*i.e.*, five electrons indicative of NO^0, six of NO^-, four of NO^+). Thus, collective weights of various resonance structures reported in this study (Table 3, main article) sum up to 100% within round-off error.

Note that in the present analysis the σ_{NO} orbital (lone pair) is not enforced to be strictly localized and it is treated within the above group (II) of orbitals. The σ_{NO} orbital, if at all involved in the Co–NO bonding, gives rise to only a weak donation of lone pair to Co d orbital(s), which is a purely classical effect, not of our direct interest in this study. Note also that due to mostly nonbonding character of the σ_{NO} orbital with respect to the N–O bond (in contrast to π^*_{NO} / π_{NO} orbitals, which have a clear antibonding / bonding character), a donation from σ_{NO} to Co is not expected to notably activate / deactivate the adsorbed NO.

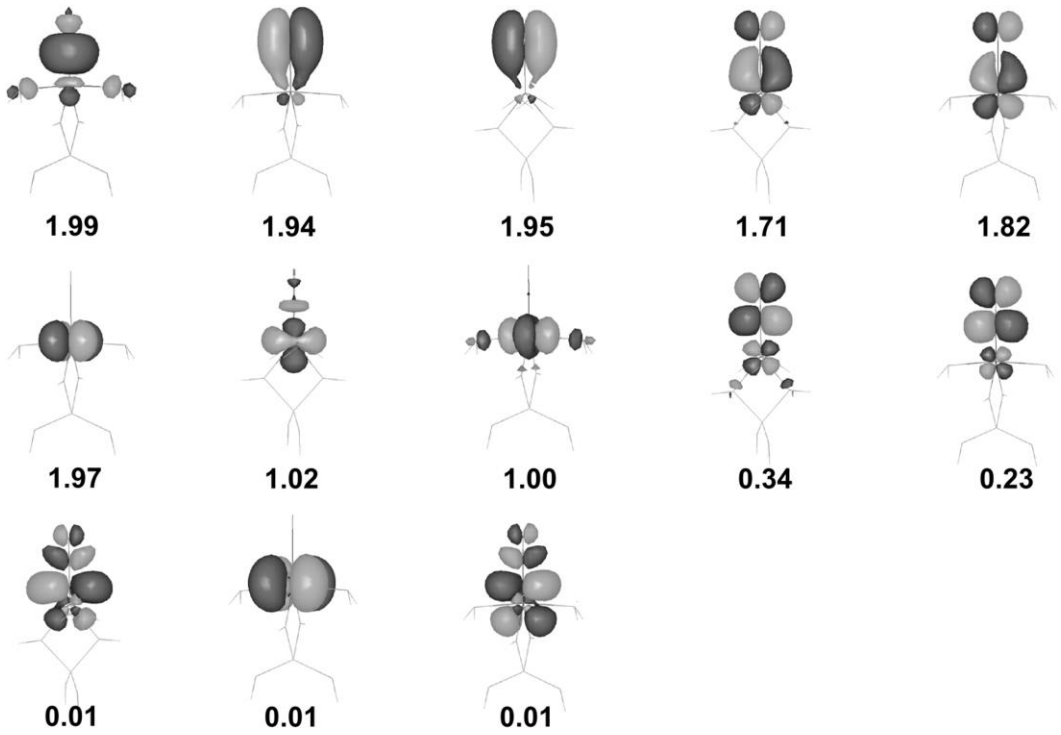

Fig. S4. CASSCF molecular orbitals and their natural occupations for triplet $[(T1)Co(H_2O)_2NO]^+$ adduct ($\mathbf{(a)_T}$); black – positive contour, grey – negative contour (contour value ±0.04 a.u.)

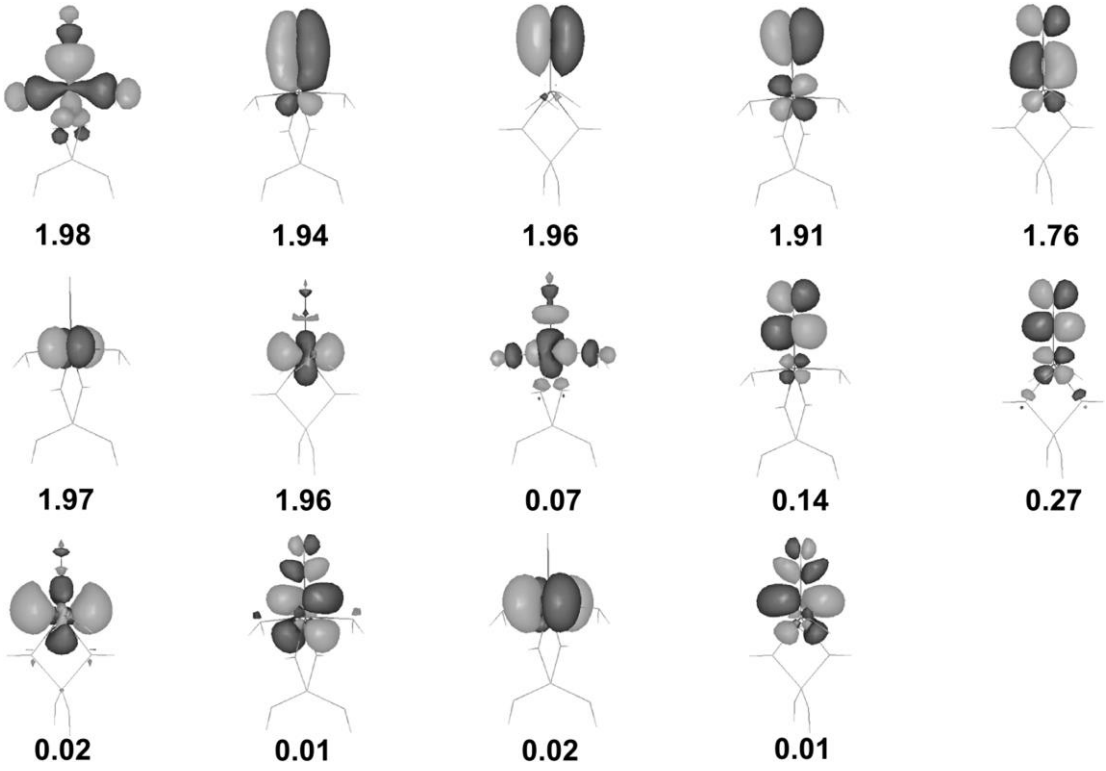

Fig. S5. CASSCF molecular orbitals and their natural occupations for singlet $[(T1)Co(H_2O)_2NO]^+$ adduct (**(a)$_S$**); black – positive contour, grey – negative contour (contour value ±0.04 a.u.)

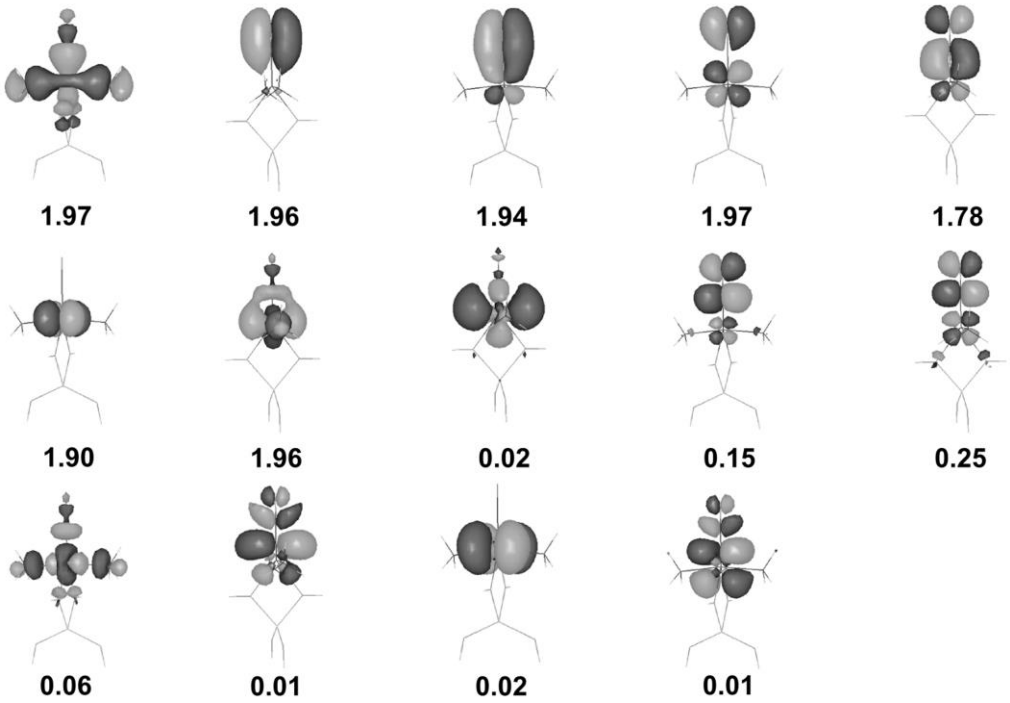

Fig. S6. CASSCF molecular orbitals and their natural occupations for singlet $[(T1)Co(NH_3)_2NO]^+$ adduct (**(a*)$_S$**); black – positive contour, grey – negative contour (contour value ±0.04 a.u.)

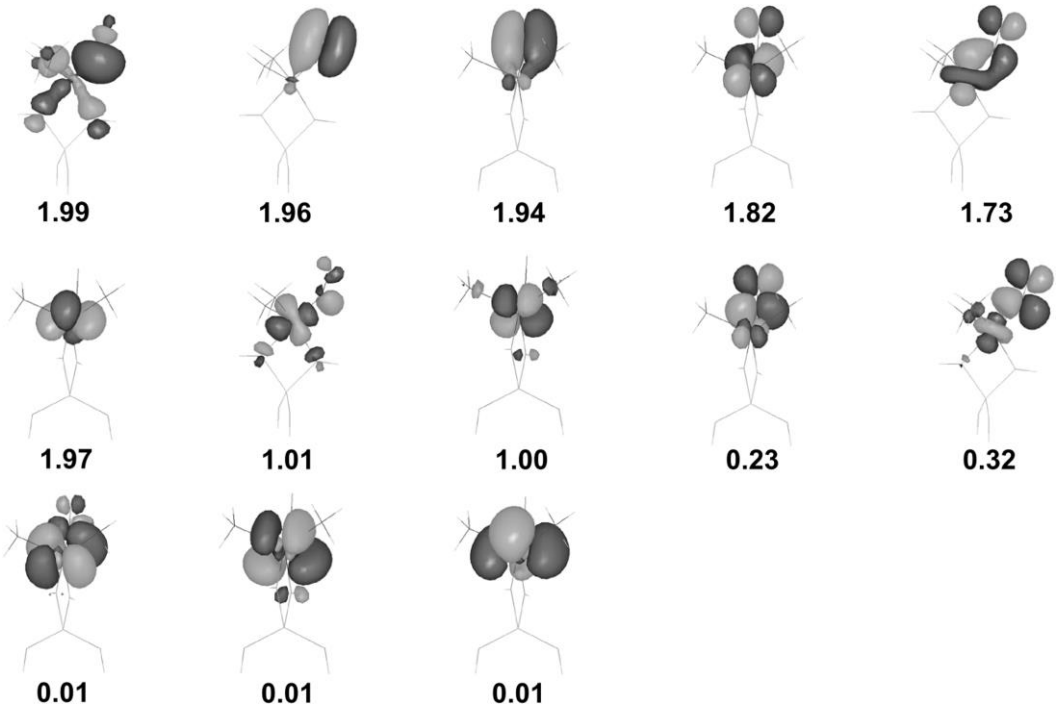

Fig. S7. CASSCF molecular orbitals and their natural occupations for triplet $[(T1)Co(NH_3)_2NO]^+$ adduct (**$(a^*)_T$**); black – positive contour, grey – negative contour (contour value ±0.04 a.u.)

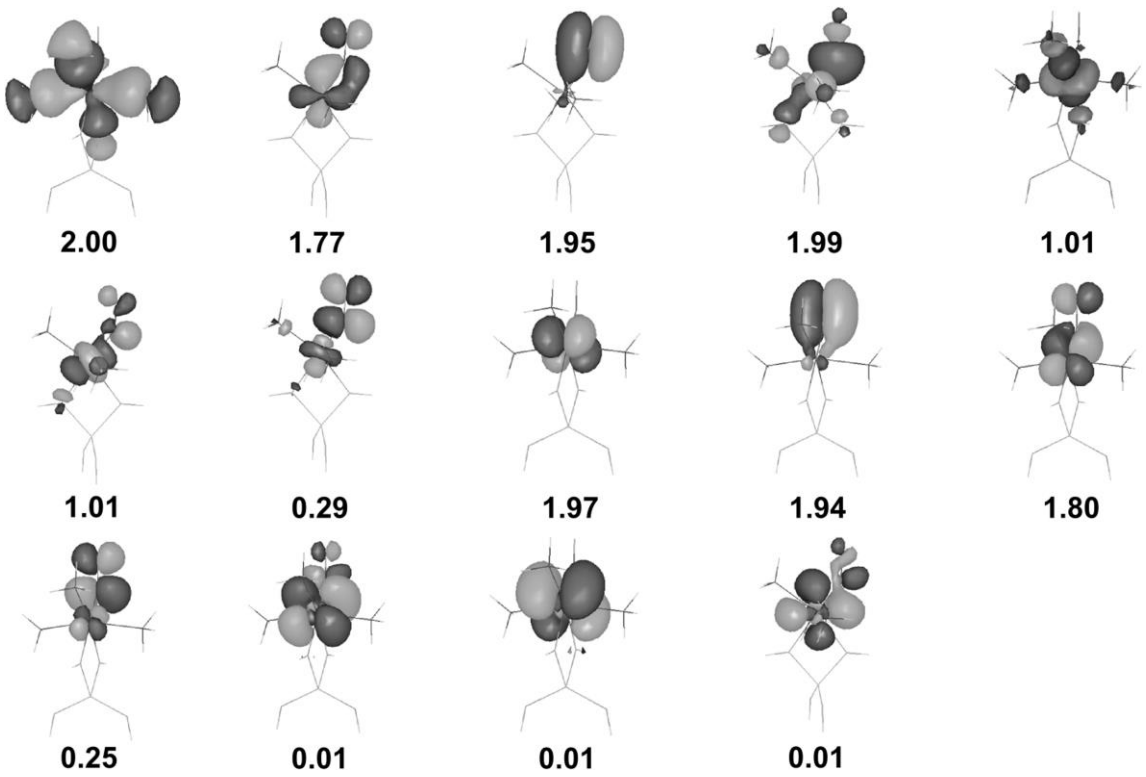

Fig. S8. CASSCF molecular orbitals and their natural occupations for triplet **(b)$_T$** adduct $[(T1)Co(NH_3)_3NO]^+$; black – positive contour, grey – negative contour (contour value ±0.04)

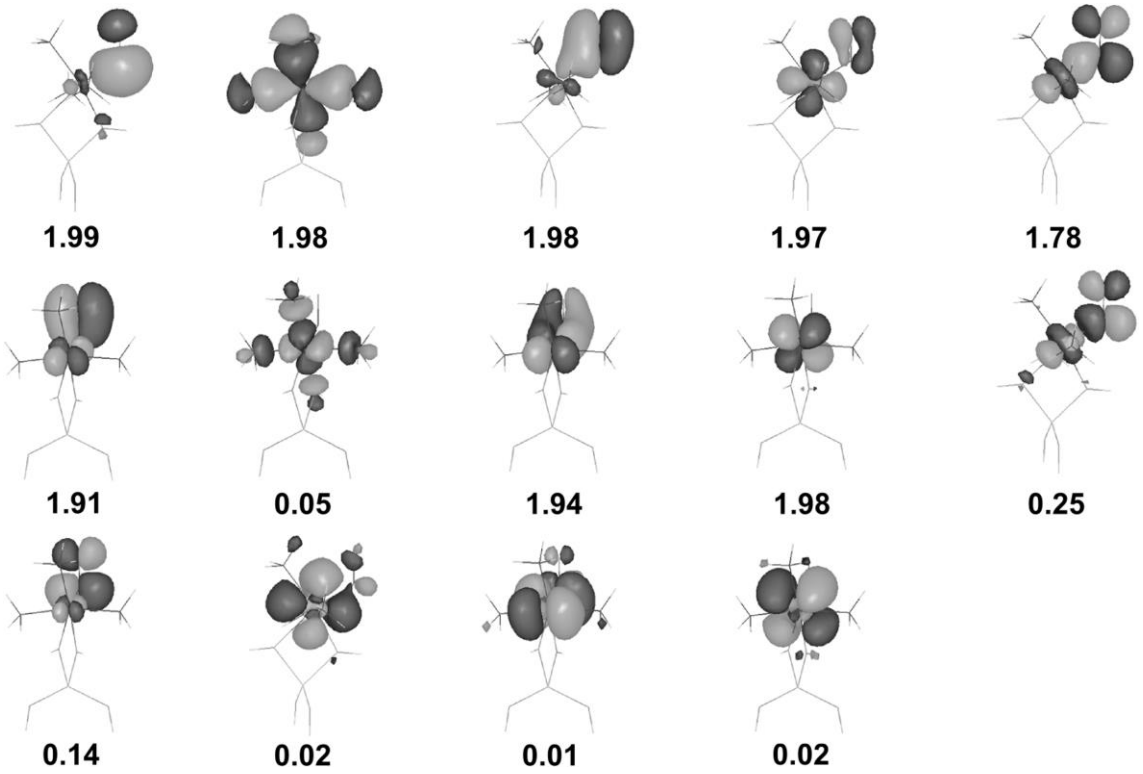

Fig. S9. CASSCF molecular orbitals and their natural occupations for singlet $[(T1)Co(NH_3)_3NO]^+$ adduct (**(b)$_S$**); black – positive contour, grey – negative contour (contour value ±0.04).

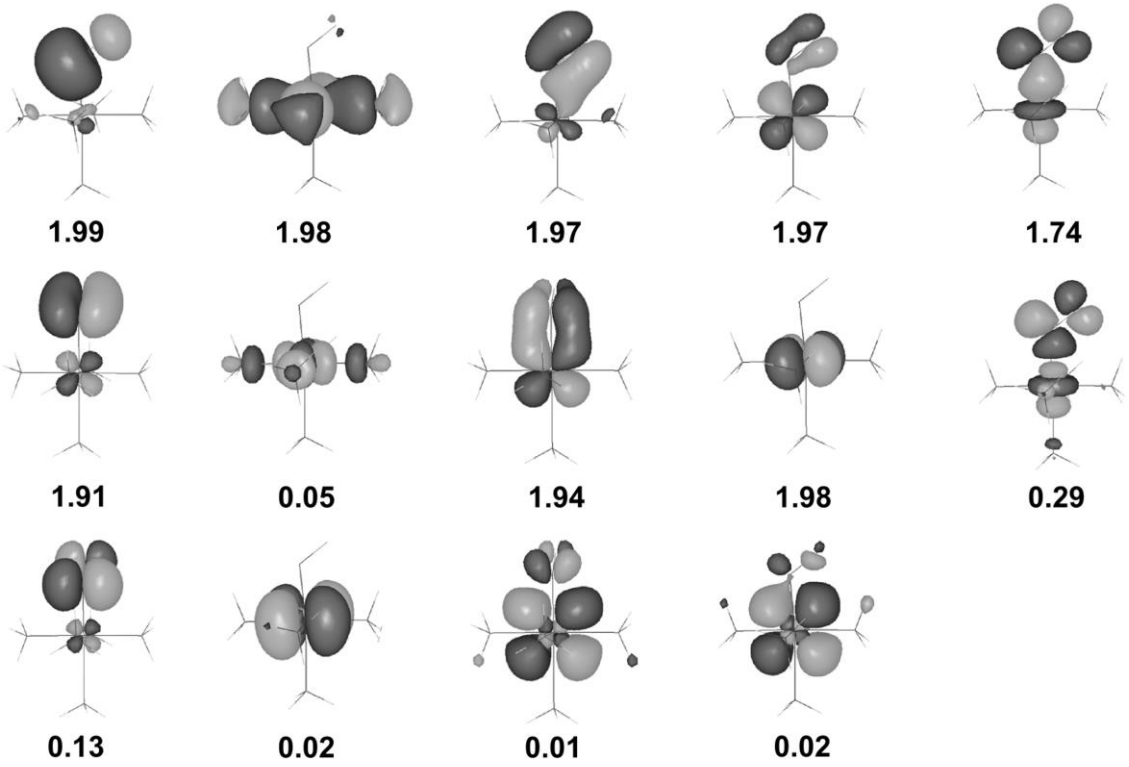

Fig. S10. CASSCF molecular orbitals and their natural occupations for singlet $[Co(NH_3)_5NO]^{2+}$ complex (**(c)$_S$**); black – positive contour, grey – negative contour (contour value ±0.04).

III. UDFT spin orbitals for triplet systems; Dominant electron transfer channels for triplet complexes with two water or two ammonia co-ligands.

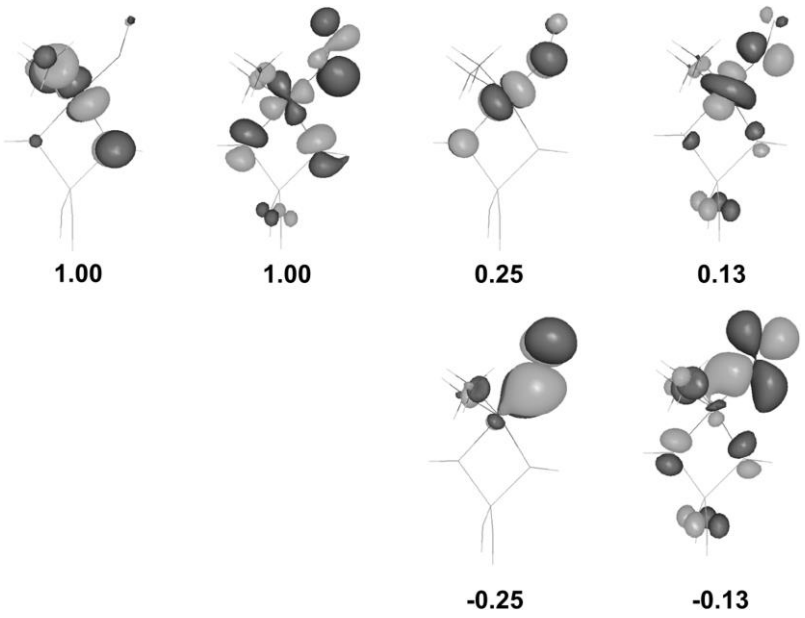

Figure S11. UDFT natural spin orbitals (NSOs) for complex **$(a^*)_T$;** two pairs with ±λ eigenvalues correspond to weakly coupled α and β electrons; black – positive contour, grey – negative contour (contour value ±0.04 a.u.) .

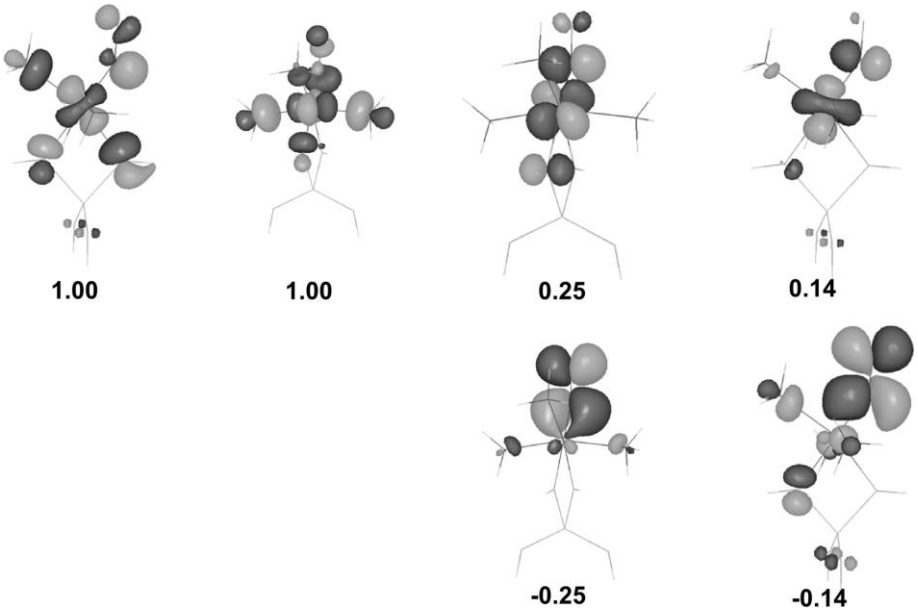

Fig. S12. UDFT natural spin orbitals (NSOs) for triplet $[(T1)Co(NH_3)_3NO]^+$ adduct (**(b)$_T$**); pairs with $\pm\lambda$ eigenvalues correspond to partly uncoupled α and β electrons; black – positive contour, grey – negative contour (contour value ±0.04).

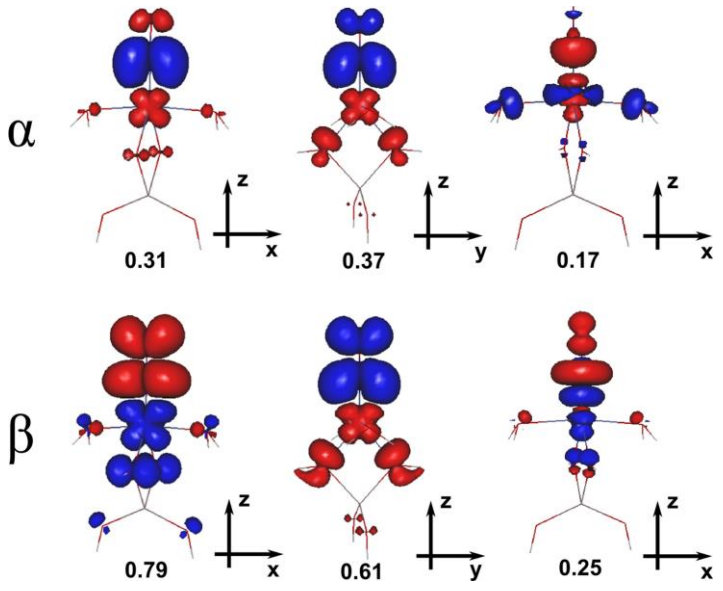

a)

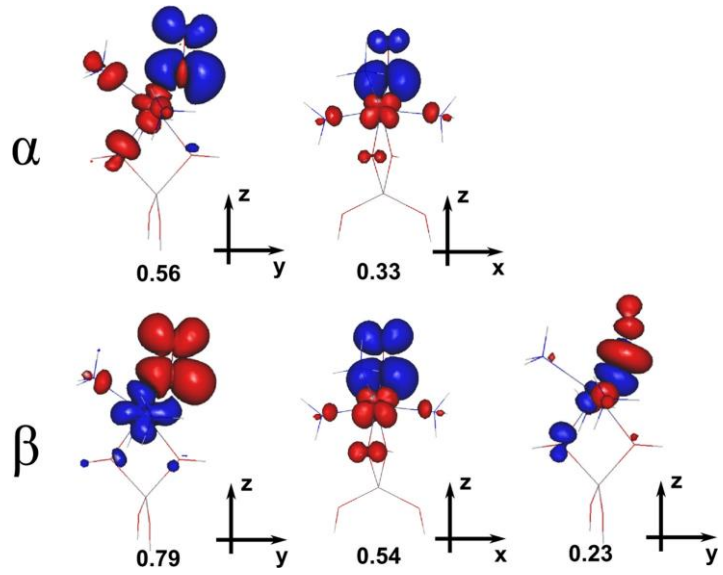

b)

Fig. S13. Dominant electron transfer channels for triplet complexes:
a) $[CoAl(OH)_4(H_2O)_2]^{2+}$- NO $\mathbf{(a)_T}$ and b) $[CoAl(OH)_4(NH_3)_3]^{+}$- NO $\mathbf{(b)_T}$ models;
red – depletion, blue – accumulation of electron density (contour value ±0.001

IV. Relative CASSCF energies of spin states, contraction of ANO-RCC basis sets and active space employed in CASSCF/CASPT2 calculations; Basis sets used in the coupled cluster calculations, relative spin-state energetics at the CCSD(T) level; Diagnostics of multireference character at the CCSD level for hexaammine complexes of Co(II) and Co(III), and models (a), (a*), (b), (c).

Table S2. Relative energy of singlet (S) and triplet (T) states for models (**a**), (**a***), (**b**), and (**c**) calculated at the CASSCF/(ANO-II) level.

Method	Relative energy (kcal/mol)							
	(a)$_S$	**(a)$_T$**	**(a*)$_S$**	**(a*)$_T$**	**(b)$_S$**	**(b)$_T$**	**(c)$_S$**	**(c)$_T$**
CASSCF	2.4	0	0	16.2	4.5	0	5.8	0

Table S3. Two contractions of the ANO-RCC basis set used in this work.

	Co	N, O	Al	H
ANO-I	6s5p3d2f1g	3s2p1d	4s3p1d	2s1p
ANO-II	10s9p8d6f4g2h	5s4p3d2f1g	5s4p2d1f	3s2p1d

Table S4. Active spaces employed in CASSCF/CASPT2 calculations in this study.

Model and spin state	Active space
$(\mathbf{a})_T$	(14,13) = A
$(\mathbf{a})_S$	(14,14) = A + $d'_{y2,Co}$
$(\mathbf{a}^*)_T$	(14,13) = A
$(\mathbf{a}^*)_S$	(14,14) = A + $d'_{y2,Co}$
$(\mathbf{b})_T$	(16,14) = A + σ_{NH3}
$(\mathbf{b})_S$	(16,14) = A + σ_{NH3}
$(\mathbf{c})_S$	(16,14) = A + σ_{NH3}
$(\mathbf{c})_T$	(16,14) = A + σ_{NH3}

Table S5. Orbital and auxiliary basis sets used in the coupled cluster calculations.

	Basis set	**Atom type**
CCSD(T), DK	cc-pwCVTZ-DK cc-pVDZ-DK	Co other atoms
CCSD(T), NR	cc-pwCVTZ cc-pVDZ	Co other atoms
CCSD(T)-F12; atomic orbital basis set	cc-pwCVTZ cc-pVTZ cc-pVDZ	Co NO and 1st coord. sphere other atoms
CCSD(T)-F12; `df_basis` density-fitting basis set	aug-cc-pVTZ/mp2fit aug-cc-pVTZ/mp2fit aug-cc-pVDZ/mp2fit	Co NO and 1st coord. sphere other atoms
CCSD(T)-F12; `df_basis_exch` density fitting basis for computing the exchange and Fock operators	def2-TZVPP/jkfit aug-cc-pVTZ/jkfit aug-cc-pVDZ/jkfit	Co NO and 1st coord. sphere other atoms
CCSD(T)-F12; `ri_basis` basis set for RI (resolution of the identity)	def2-TZVPP/jkfit aug-cc-pVTZ/optri aug-cc-pVDZ/optri	Co, Al NO and 1st coord. sphere other atoms

Table S6. Relative spin-state energetics at the CCSD(T) level[a] and diagnostics of multireference character (T_1, D_1 diagnostics) at the CCSD level[b] for hexaammine complexes of Co(II) and Co(III).

	$[Co(NH_3)_6]^{2+}$		$[Co(NH_3)_6]^{3+}$	
	S = 1/2	S = 3/2	S = 0	S = 1
$\Delta E_{CCSD(T)}$ (kcal/mol)	11.1	0[c]	0[c]	29.7
T_1 diagnostics	0.021	0.014	0.034	0.033
D_1 diagnostics	0.124	0.055	0.170	0.209

[a]See computational protocol described in the manuscript. [b]Relativistic calculations with the cc-pwCVTZ-DK (Co), cc-pVDZ-DK (all ligands) basis set. [c] ΔE = 0 for the experimentally-assigned spin state.

Table S7. Diagnostics of multireference character (T_1, D_1 diagnostics) at the CCSD level[a] and weights of the leading configuration state function (C_0^2) in the CASSCF wave function expanded in terms of natural orbitals [b] for alternative spin states of models (**a**), (**a***) and (**b**).

	$\mathbf{(a)_S}$	$\mathbf{(a)_T}$	$\mathbf{(a^*)_S}$	$\mathbf{(a^*)_T}$	$\mathbf{(b)_S}$	$\mathbf{(b)_T}$	$\mathbf{(c)_S}$	$\mathbf{(c)_T}$
T_1	0.046	0.039	0.054	0.029	0.051	0.052	0.057	0.047
D_1	0.301	0.238	0.357	0.146	0.394	0.315	0.393	0.230
C_0^2	76.2%	66.8%	76.7%	67.8%	78.0%	68.4%	76.4%	67.2%

[a] Relativistic calculations with the cc-pwCVTZ-DK (Co), cc-pVDZ-DK (all ligands) basis set.
[b] Relativistic calculations with ANO-I basis set.

Additional References

S1. G. Kresse and J. Hafner, *Phys. Rev. B*, 1993, 48, 13115.

S2. G. Kresse and J. Hafner, *Phys. Rev. B*, 1994, 49, 14251.

S3. G. Kresse and J. Furthmüller, *Comput. Mater. Sci.*, 1996, 6, 15.

S4. G. Kresse and J. Furthmüller, *Phys. Rev. B*, 1996, 54, 11169.

S5. P. Blöchl, *Phys. Rev. B*, 1994, 50, 17953.

S6. G. Kresse and D. Joubert, *Phys. Rev. B*, 1999, 59, 1758.

S7. J.P. Perdew, K. Burke and M. Ernzerhof, *Phys. Rev. Lett.*, 1996, 77, 3865–3868.

S8. W.H. Press, B.P. Flannery, S.A. Teukolsky and W.T. Vetterling, *Numerical Recipes in FORTRAN 77: The Art of Scientific Computing*, second ed., vol. 1, Cambridge University Press, 1992.

S9. S.I. Zones and R.A. Van Nostrand, *Zeolites*, 1988, 8, 166.

S10. J. Dedecek, Z. Sobalik and B. Wichterlova, *Catalysis Reviews: Science and Engineering*, 2012, 54, 135-223

S11. J. Dedecek, D. Kaucky, B. Wichterlova and O. Gonsiorova, Phys. *Chem. Chem. Phys.*, 2002, 4, 5406-5413

S12. J.Dedecek, D. Kaucky and B. Wichterlova, *Chem. Commun.*, 2001, 970-971

S13. J. Pipek and P.G. Mezey. *J. Chem. Phys.*, 1989, 90, 4916.